

Connected Network Model for the Mechanical Loss of Amorphous Materials

Steven Blaber,^{1,*} Daniel Bruns,¹ and Jörg Rottler^{1,†}

¹*Dept. of Physics and Astronomy and Stewart Blusson Quantum Matter Institute, University of British Columbia, Vancouver, British Columbia V6T 1Z1, Canada*

Mechanical loss in amorphous solids at low frequencies is commonly attributed to thermally activated transitions of isolated two-level systems (TLS) that come in resonance with a mechanical wave. Using atomistic modeling of amorphous silicon, we observe instead that the inherent structures that constitute the TLS form a sparsely connected network with thermodynamic pathways between states. An analytically tractable theory for mechanical loss of the full network is derived from a nonequilibrium thermodynamic perspective. We show that the connected network model predicts mechanical loss with distinct temperature and frequency profiles when compared to the isolated TLS model. This not only calls into question the validity of the TLS model, but also gives us many new avenues and properties to analyze for the targeted design of low mechanical loss materials for applications in gravitational wave detectors.

Introduction.—For over 50 years, the two-level system (TLS) model has stood as the prevailing description of thermal and acoustic properties of amorphous solids [1–3]. This is in part due to its success in predicting the linear scaling heat capacity and quadratic scaling of the thermal conductivity in the low temperature tunneling regime [3–5]. TLS are also believed to contribute to mechanical dissipation in amorphous mirror coatings [6], which is currently a critical factor limiting the sensitivity of interferometer-based gravitational wave detectors (GWD) [7]. TLS also contribute to the dielectric loss of quantum materials (e.g. superconducting qubits [8–10]) and a better understanding is vital to the field of cavity optomechanics [11], which has applications to quantum memory, high precision sensors, and quantum transducers.

Amorphous materials are intrinsically disordered, which results in characteristically rugged and complex energy landscapes that make their properties notoriously difficult to predict [3]. At thermal equilibrium, the material can occupy and transition between many distinct *inherent structures*: stable minima of the energy landscape. In the TLS model (Fig. 1), pairs of inherent structures connected by a transition path are driven out of equilibrium by acoustic vibrations resulting in internal friction and mechanical loss [3, 4, 12]. Each TLS is assumed to be independent and equally likely to be occupied, and the resultant loss of the material is the superposition of the individual contributions from each TLS. Within the TLS model, there are two important parameters: the energy barrier and the energy asymmetry between the two inherent structures. The former determines the timescale of the TLS and the frequency at which it can be excited, while the latter determines the magnitude of the mechanical loss (low asymmetry results in high mechanical loss).

The TLS model has been used to study the mechanical loss of several candidate materials for GWD coatings [12–17]. Of particular relevance are studies of amorphous silicon [13, 18–22], silica [12, 15], and tantalum [17, 23]. These studies have given us key insights into the nature,

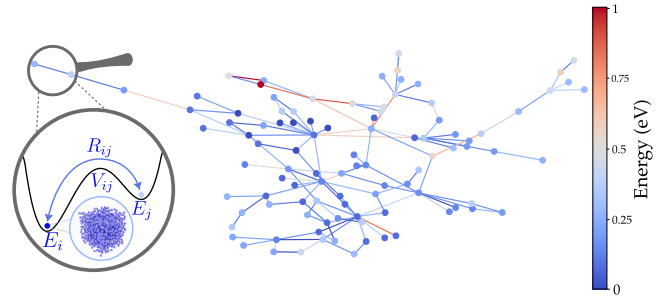


FIG. 1. First 100 nodes of the connected network of inherent structures observed in a sample of amorphous silicon. Inset: TLS model between inherent structures (i, j) with energy minima E_i and energy barrier V_{ij} . The inherent structures are coarse-grained to discrete states with transition rates R_{ij} between states. The color of the dots and lines correspond to the energy of the minima E_i and the average barrier height $V_{ij} - (E_i + E_j)/2$ respectively.

atomic structure, and motion of TLS in these materials. Over the years, several of the common assumptions made in estimates of mechanical loss from TLS have been addressed and improved upon, e.g. assumptions on the distributions and independence of energy barriers and asymmetries [12, 15].

Despite these improvements, the TLS model still provides a highly simplified description of amorphous materials. Specifically, it assumes that all the TLS are independent, ignoring the rugged and high dimensional nature of the energy landscape. In our atomistic simulations, we test this assumption and find that the system does not consist of independent TLS but instead forms a connected network of inherent structures (Fig. 1), calling into question the predictions of the TLS model. To address the mechanical loss of the connected network, we take a nonequilibrium thermodynamic perspective [24]: modeling the heat dissipated from a driven process using master equation dynamics [25] of the discrete state network.

Nonequilibrium Thermodynamics.—Mechanical loss of

a material relates to the decay of acoustic vibrations due to internal energy dissipation. With each oscillation, energy is dissipated as heat $\mathcal{Q}_{\text{cycle}}$ into the environment, which is compared to the stored elastic energy through the inverse *quality factor*

$$Q^{-1} = \frac{1}{2\pi} \frac{\mathcal{Q}_{\text{cycle}}}{\text{energy stored}}. \quad (1)$$

This relation allows us to relate the quality factor to the dissipated heat, which can then be used to estimate the quality factor based on material properties.

We separate the total energy of the system into the elastic energy of the acoustic wave of frequency ω traveling through the material and the internal energy of the connected network of inherent structure as $\mathcal{U}_{\text{tot}} = \mathcal{U}_{\text{elastic}} + \mathcal{U}_{\text{CN}}$. Assuming an isotropic and linear elastic material with oscillating strain $\epsilon(t) = \epsilon_0 \sin(\omega t)$, the elastic energy is

$$\mathcal{U}_{\text{elastic}}(t) = \mathcal{V} C \epsilon_0^2 \sin^2(\omega t), \quad (2)$$

for volume \mathcal{V} and elastic modulus C (longitudinal or shear). The macroscopic energy input of the entire material oscillating under strain averaged over one cycle is $\mathcal{V} C \epsilon_0^2 / 2$.

The strain couples to the energy of the inherent structures \mathbf{E} as

$$\mathbf{E}(t) = \mathbf{E}(0) + \left(\alpha \mathbf{1} + \frac{\epsilon_0 \gamma_0}{2} \mathbf{\Gamma} \right) \sin(\omega t), \quad (3)$$

where $\mathbf{1}$ is a vector of ones and throughout a bold symbol represent a vector with elements spanning the inherent structures; i.e. E_i is the energy of inherent structure i . The coupling between the inherent structure and applied strain is separated into a constant term α and an inherent structure dependent term $\mathbf{\Gamma}$ with amplitude γ_0 . The constant term will not affect the dynamics since it will affect all energies equally. The average energy of the network is the number of inherent structures N times the average energy per inherent structure

$$\mathcal{U}_{\text{CN}}(t) = N \mathbf{P}_t \cdot \mathbf{E}(t), \quad (4)$$

with \mathbf{P}_t the time dependent inherent structure occupation probability.

The rate of change in energy gives the first law of thermodynamics

$$\dot{\mathcal{U}}(t) = \dot{\mathcal{W}}(t) + \dot{\mathcal{Q}}(t), \quad (5)$$

with the work resulting from changes in energy

$$\dot{\mathcal{W}} = \dot{\mathcal{U}}_{\text{elastic}} + N \mathbf{P}_t \cdot \dot{\mathbf{E}}(t), \quad (6)$$

and the heat from the time dependent probabilities

$$\dot{\mathcal{Q}} = N \dot{\mathbf{P}}_t \cdot \mathbf{E}(t). \quad (7)$$

Throughout, a dot denotes the rate of change with respect to time. The work and heat produced in a cyclic process are $\mathcal{W}_{\text{cycle}} = \int_{\text{cycle}} dt \dot{\mathcal{W}}$ and $\mathcal{Q}_{\text{cycle}} = \int_{\text{cycle}} dt \dot{\mathcal{Q}}$. For a cyclic process in a periodic steady-state $\Delta \mathcal{U}_{\text{cycle}} = 0$ so $\mathcal{Q}_{\text{cycle}} = -\mathcal{W}_{\text{cycle}}$.

We describe the dynamics of the system by a *master equation*, which is a discrete state model that describes conservation of probabilities as they transition between states [25]

$$\frac{d\mathbf{P}_t}{dt} = R(t) \mathbf{P}_t, \quad (8)$$

with a transition rate matrix $R(t)$. For a system at inverse temperature $\beta \equiv (k_B T)^{-1}$ with temperature T and Boltzmann constant k_B , the transition rates are expressed as Arrhenius rates in terms of the energy barriers V_{ij} and energy levels E_i of the inherent structures i and j , so the transition rate matrix has elements

$$R_{ij} = k_{ij} e^{\beta E_j} \left[e^{-\beta V_{ij}} (1 - \delta_{ij}) - \delta_{ij} \sum_{\ell \neq j} e^{-\beta V_{j\ell}} \right]. \quad (9)$$

Due to the exponential dependence, the transition rates are dominated by the barrier heights V_{ij} rather than the bare transition rates k_{ij} [23]. For simplicity, we assume equal bare transition rates $k_{ij} = k_0$ for all transitions in our numerical calculations, an assumption made in a previous study [13] and supported by atomistic simulations of amorphous silicon [26].

Connected Network Model.—Although the equations of the previous section (Eq. (7) and Eq. (8)) are sufficient to determine the energy dissipation and hence the mechanical loss of the system, considerable simplification can be made if we assume the amplitude of oscillations are small. This is consistent with the small amplitude assumption made in the TLS model [12] and should be sufficient for applications to GWD where the magnitude of vibrations in the system are extremely small [7].

For small amplitude oscillations $\beta \epsilon_0 \gamma_0 \equiv \tilde{\gamma}_0 \ll 1$, we expand the probabilities around their static equilibrium values $P_i^{\text{eq}} = e^{-\beta E_i} / \sum_j e^{-\beta E_j}$ as

$$\mathbf{P}_t = \mathbf{P}^{\text{eq}} + \tilde{\gamma}_0 \mathbf{P}_t^{(1)} + \mathcal{O}(\tilde{\gamma}_0^2), \quad (10)$$

with $\mathbf{P}_t^{(1)}$ denoting the contribution of order $\tilde{\gamma}_0$ defined by the above expansion. Similarly, expanding Eq. (9) about its static value $R = R^{(0)} + \tilde{\gamma}_0 R^{(1)}(t) + \mathcal{O}(\tilde{\gamma}_0^2)$ we have

$$R_{ij}^{(1)}(t) = \frac{1}{2} R_{ij}^{(0)} \mathbf{\Gamma}_j \sin(\omega t). \quad (11)$$

Substituting into Eq. (8) leads to

$$\frac{\partial \mathbf{P}_t^{(1)}}{\partial t} \simeq R^{(0)} \mathbf{P}_t^{(1)} + R^{(1)}(t) \mathbf{P}^{\text{eq}}. \quad (12)$$

In a periodic steady state this has the solution

$$\begin{aligned} \mathbf{P}_t^{(1)} &= -\frac{\beta\epsilon_0\gamma_0}{2} [\mathbf{A}\sin(\omega t) + \mathbf{B}\cos(\omega t)] \quad (13) \\ A_i &\equiv \sum_{jk} M_{ij} \frac{1}{1 + (\omega\tau_j)^2} M_{jk}^{-1} \Gamma_k P_k^{\text{eq}} \\ B_i &\equiv \sum_{jk} M_{ij} \frac{\omega\tau_j}{1 + (\omega\tau_j)^2} M_{jk}^{-1} \Gamma_k P_k^{\text{eq}}. \end{aligned}$$

The relaxation times τ_j are related to the eigenvalues λ_j of $R^{(0)}$ as $\tau_j \equiv \lambda_j^{-1}$ with corresponding eigenvectors forming the columns of the eigenvector matrix M .

Substituting Eqs. (10) and Eq. (13) into Eq. (7), then integrating over one cycle, we arrive at our central result

$$\mathcal{Q} = \frac{\beta\pi N\epsilon_0^2\gamma_0^2}{4} \sum_{i,j,\ell} \Gamma_i M_{ij} \frac{\omega\tau_j}{[1 + (\omega\tau_j)^2]} M_{j\ell}^{-1} \Gamma_\ell P_\ell^{\text{eq}}. \quad (14)$$

The energy dissipation is decomposed into contributions from eigenmodes of the transition matrix R , each contributing to the overall mechanical loss. Since R is a transition rate matrix of a connected network, it has exactly one zero eigenvalue with eigenvector corresponding to the equilibrium distribution. All other eigenvalues are negative (describing relaxation towards equilibrium) with eigenvectors that sum to zero (preserves normalization of probability).

We assume the total energy stored in the system (averaged over one cycle) is dominated by the elastic energy (2), so the inverse quality factor (1) is

$$Q^{-1} = \frac{\beta N\gamma_0^2}{4\mathcal{V}C} \sum_{i,j,\ell} \Gamma_i M_{ij} \frac{\omega\tau_j}{[1 + (\omega\tau_j)^2]} M_{j\ell}^{-1} \Gamma_\ell P_\ell^{\text{eq}}. \quad (15)$$

For an alternate derivation of this result, see Supplemental Material I.

The TLS model corresponds to a network where every pair of inherent structures are isolated. For this network there is no global equilibrium and each pair of connected inherent structures must be treated independently. In Supplemental Material II, we calculate the quality factor for a network of two inherent structures, which when summed over all independent pairs yields a quality factor consistent with the popular TLS model [12]

$$Q_{\text{TLS}}^{-1} = \frac{\beta}{4\mathcal{V}C} \sum_i \gamma_i^2 \text{sech}^2\left(\frac{\beta\Delta_i}{2}\right) \frac{\omega\tau_i}{1 + \omega^2\tau_i^2}, \quad (16)$$

with Δ_i the energy difference between the two inherent structures in TLS i , $\gamma_i = \gamma_0\Gamma_i$ the TLS deformation potential, and TLS relaxation time

$$\tau_i = \frac{e^{\beta V_i}}{k_0(1 + e^{\beta\Delta_i})}. \quad (17)$$

Connectivity of Inherent Structures.—We perform molecular dynamics simulations of amorphous silicon using a Tersoff potential [27] in LAMMPS [28]. We prepare samples via melt-quench at a quench rate of $10^{11}K/s$ and find inherent structures by thermal search trajectories at $600K$ for 200ps with a sampling frequency of 100fs. We determine candidate TLS based on changes in the minimum energy and filter them based on participation ratio and maximum atomic displacement to remove unlikely candidates. Duplicate pairs of TLS are determined and removed based on a root-mean-squared atomic displacement criterion between structures less than 10^{-4}\AA . This procedure is common for amorphous sample preparation [29] and TLS calculations from MD simulation [12, 13]. We add an additional step in our analysis and use the same method for removing duplicate TLS to determine which inherent structures are identical. In this way, we connect TLS together (e.g. TLS A-B and B-C becomes A-B-C), thus forming connected networks of inherent structures as shown in Fig. 1. Typically we find networks of $\sim 1000 - 3000$ inherent structures. Further simulation details can be found in Supplemental Material III.

We find the statistical properties of the networks to be robust between samples. Figure 2a shows the percentage of the network that is connected (number of connections/total number of possible connections) as a percentage of the full network. The percentage of the network that is connected plateaus around $\sim 0.05\%$ as the entire sample is included with negligible variation between samples, indicating a sparsely connected network.

The fraction of cycles (connected loops of inherent structures) of a given size has relatively small variation between samples (Fig. 2c). Cycles are of particular interest since they cannot be reproduced by the TLS model. Each cycle presents an alternate pathway between states: a chain of states with a cycle in the middle has two pathways to travel from end-end, potentially allowing the system to avoid large energy barriers. Interestingly, we find no odd-state cycles, hinting at some intriguing physics underpinning the networks, and future studies are needed to reveal if this property is unique to amorphous silicon.

The observed degree (i.e. the number of connections of an inherent structure) distribution has a power law form (Fig. 2b), indicating that the inherent structure form a scale-free network. Scale-free networks have also been observed in Lennard-Jones clusters [30]. However, we have not completed an exhaustive search of all inherent structures, and the power-law scaling could arise from preferential sampling of nodes connected to the initial inherent structure and those with high degree (many connections).

The relative eccentricity of a node measures the (minimum) number of steps required to reach the furthest node relative to the number of nodes. Since the networks typically consist of $1000 - 3000$ inherent structures, the observed relative eccentricity $\lesssim 0.03$ indicates it takes rel-

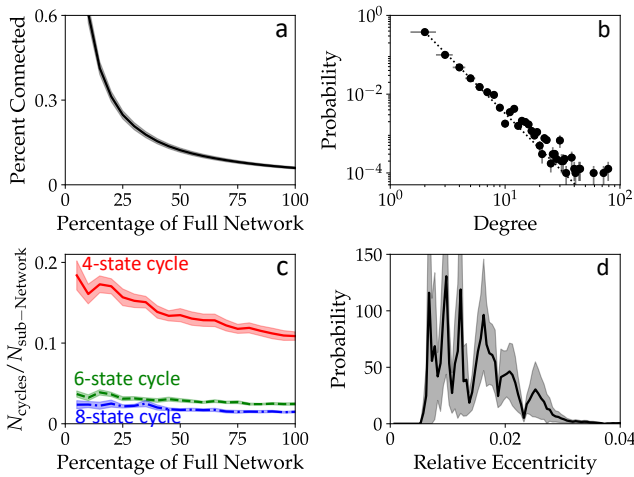


FIG. 2. Statistical properties of the connected networks of inherent structures of amorphous silicon. a) Percentage of the network that is connected $100\% \times N_{\text{connected}}/N_{\text{sub-Network}}^2$ as a function of the percentage of the full network $100\% \times N_{\text{sub-Network}}/N_{\text{tot}}$. b) Probability distribution of the degree (number of connection) of nodes in the network with the dotted line a linear least squares fit with a slope (scaling exponent) of -2.95 ± 0.04 . c) Fraction of the number of basis cycles of each size (4 nodes: red solid, 6 nodes: green dashed, and 8 nodes: blue dash-dotted) as function of the percentage of nodes in the sub-network. d) Probability distribution of the relative eccentricity (minimum number of steps to reach the furthest node / number of nodes). Error bars and shaded region indicate one standard error of the mean.

atively few steps to cross the entire network, a property commonly referred to as “small world” [31].

Mechanical Loss.—Several properties of the mechanical loss can be inferred directly from Eq. (15). For low frequencies $\omega\tau \ll 1$ the mechanical loss Eq. (15) scales as ω , while for high frequencies $\omega\tau \gg 1$ it scales as ω^{-1} . In the intermediate regime there is a plateau region with peaks corresponding to $\omega\tau_j \sim 1$ for the relaxation modes that dissipate significant energy.

To estimate the mechanical loss of amorphous silicon, we use a typical value for the elastic modulus $C = 50\text{GPa}$ [18, 32, 33], bare transition rate $k_0 = 10^{13}\text{s}^{-1}$ [13, 26], and estimate the deformation potential from differences in stress between connected inherent structures [12] as outlined in Supplemental Material III. We emphasize that these assumption are made for calculations within both the TLS and connected network models, and changing the value of k_0 merely leads to an overall shift in the frequency ω .

The inverse quality factor estimated from the connected network and TLS models have several qualitative and quantitative differences (Fig. 3). Within the frequency range relevant for gravitational wave detection, the network model predicts nonmonotonic behavior and a peak at $\sim 1\text{Hz}$ at 100K and 200K not present in the

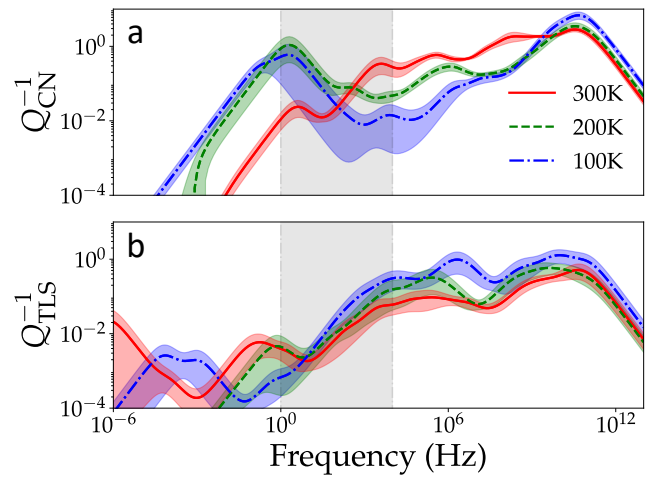


FIG. 3. Average longitudinal component of the inverse quality factor from 10 samples of amorphous silicon at $T = 300\text{K}$ (red circle/solid line), 200K (green square/dashed line), and 100K (blue triangle/dash-dotted line). a) Connected network (CN) model (15). b) TLS model (16). Shaded area around the curves is the standard error of the mean and the grey shaded region highlights the relevant frequency range for GWDs (1Hz – 10kHz). We have assumed $k_0 = 10^{13}\text{s}^{-1}$, $C = 50\text{GPa}$, and calculated $\mathcal{V} = 2.064 \times 10^{-26}\text{m}^3$.

TLS model, while the TLS model predicts several smaller peaks at frequencies below 1Hz that are not present in the network model. The network model has a global energy scale and accounts for the relative occupation probability of each inherent structure, so TLS predicted to contribute significant mechanical loss may be unlikely to be occupied in the network model due to their high relative energy, resulting in a small contribution to the mechanical loss of the network. Additionally, the topology of the connected network results in distinct relaxation modes (eigenvectors of the transition rate matrix R and their associated relaxation times τ) not possible in the TLS model and allows the system to circumvent large barriers (which cause low frequency peaks) through alternate pathways. For example, the cycles found in the network (Fig. 2) are topologically distinct from a TLS and therefore are not well represented by isolated TLS.

We quantify how many elements of the eigenvectors and how many eigenmodes significantly contribute to the total mechanical loss by the *participation ratio* (PR), which for a quantity D with elements D_i is defined as

$$D_{\text{PR}} \equiv \frac{\sum_i D_i^2}{\sum_j D_j^4}. \quad (18)$$

At a given frequency, relatively few modes dominate (mechanical loss participation ratio $\lesssim 12$, see Fig. 4a) and the relaxation modes of the connected network typically involve relatively few inherent structures (eigenvector participation ratio $\lesssim 30$ in Fig. 4 b). Although the

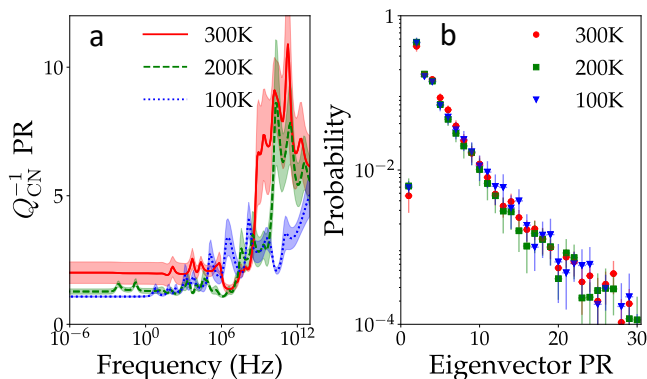


FIG. 4. Summary of properties of 10 samples of amorphous silicon at $T = 300K$ (red circle/solid line), $200K$ (green square/dashed line), and $100K$ (blue, dotted line and triangle markers). The curves/dots are averages over the samples and shaded regions/error-bars are the standard error of the mean. a) Mechanical loss participation ratio (18) (PR of Q_j^{-1} for eigenmode j) and b) eigenvector participation ratio (PR of eigenvector v_j with elements j).

dissipation and relaxation times of the collective modes of the network are distinct from the TLS, they are constrained to relatively few inherent structures. However, since the eccentricity of the network is small, they may still span the entire network.

Discussion.—We have observed a connected network of inherent structures coupled by thermally activated transitions in samples of amorphous silicon. The connected network structure challenges the assumption of the TLS model that pairs of structures can be treated independently. We find robust network properties across 10 independent samples (Fig. 2): the networks are relatively sparsely connected ($\sim 0.05\%$), the degree distribution has power law scaling, a significant fraction of even-state cycles are present, and the eccentricity of the networks shows relatively few jumps are required to cross the entire network.

To address the mechanical loss of the full connected network, we develop an analytical model from a nonequilibrium thermodynamic perspective: the dynamics of the discrete state network of inherent structures is described by the master equation (8) for the time dependent probabilities, ultimately leading to an explicit expression for the energy dissipated in a single cycle of an acoustic oscillation (7). The connected network model generalizes the standard TLS description (Fig. 3). We find that the connected network and TLS models have a qualitatively distinct frequency spectrum. The decomposition of the heat into eigenmodes shows that few modes $\lesssim 12$ dominate at any given frequency and within each mode only a few elements of the eigenvector significantly contribute $\lesssim 30$.

A major advantage of the network structure is that it provides new properties to analyze in order to improve

our physical understanding of internal friction in amorphous materials, potentially revealing new methods for the design of low mechanical loss coatings. Future studies may reveal which network properties can be related to changes in mechanical loss. Additionally, the robust nature of the statistical network properties opens up the possibility for the discovery of universal features of amorphous materials. One good candidate is the scale free degree distribution, which has been observed in similar materials [30].

The significant quantitative and qualitative differences between the connected network and TLS models call for a re-examination of earlier TLS model predictions. Of particular interest is the effect of aging and annealing on mechanical loss, which has been the subject of several recent studies [16, 17, 34, 35]. Annealing has been shown to have a significant effect on mechanical loss, and it will be interesting to see how it manifests in the network structure of the material.

Although the transition rates in our model and mechanical loss calculations are restricted to classical (stochastic) dynamics, the network itself makes no such assumption. It will be interesting to see if a similar model can be used to describe connected networks of tunneling transitions at low temperature, and what implications it would have for the tunneling TLS model [3]. This is an important question as low temperature TLS are believed to be a main cause of dielectric loss in quantum materials [8–10].

This research was supported in part by the Canada First Research Excellence Fund, Quantum Materials and Future Technologies Program. Computational resources and services were provided by Advanced Research Computing at the University of British Columbia and the Digital Research Alliance of Canada (alliancecan.ca).

* steven.blaber@ubc.ca

† jrottler@physics.ubc.ca

- [1] W. A. Phillips, Tunneling states in amorphous solids, *Journal of low temperature physics* **7**, 351 (1972).
- [2] P. W. Anderson, B. I. Halperin, and C. M. Varma, Anomalous low-temperature thermal properties of glasses and spin glasses, *Philosophical Magazine* **25**, 1 (1972).
- [3] L. Berthier and D. R. Reichman, Modern computational studies of the glass transition, *Nature Reviews Physics* **5**, 102 (2023).
- [4] W. A. Phillips, Two-level states in glasses, *Reports on Progress in Physics* **50**, 1657 (1987).
- [5] X.-Y. Gao, H.-Y. Deng, C.-S. Lee, J.-Q. You, and C.-H. Lam, Emergence of two-level systems in glass formers: a kinetic monte carlo study, *Soft Matter* **18**, 2211 (2022).
- [6] B. P. Abbott, R. Abbott, T. Abbott, S. Abraham, F. Acernese, K. Ackley, C. Adams, R. Adhikari, V. Adya, C. Affeldt, *et al.*, Gwtc-1: a gravitational-wave transient

- catalog of compact binary mergers observed by ligo and virgo during the first and second observing runs, *Physical Review X* **9**, 031040 (2019).
- [7] J. Steinlechner, Development of mirror coatings for gravitational-wave detectors, *Philosophical Transactions of the Royal Society A: Mathematical, Physical and Engineering Sciences* **376**, 20170282 (2018).
- [8] L.-C. Ku and C. Y. Clare, Decoherence of a josephson qubit due to coupling to two-level systems, *Physical Review B* **72**, 024526 (2005).
- [9] C. Müller, J. H. Cole, and J. Lisenfeld, Towards understanding two-level-systems in amorphous solids: insights from quantum circuits, *Reports on Progress in Physics* **82**, 124501 (2019).
- [10] Y. Cho, D. Jasrasaria, K. G. Ray, D. M. Tennant, V. Lordi, J. L. DuBois, and Y. J. Rosen, Simulating noise on a quantum processor: interactions between a qubit and resonant two-level system bath, *Quantum Science and Technology* **8**, 045023 (2023).
- [11] M. Aspelmeyer, T. J. Kippenberg, and F. Marquardt, Cavity optomechanics, *Reviews of Modern Physics* **86**, 1391 (2014).
- [12] T. Damart and D. Rodney, Atomistic study of two-level systems in amorphous silica, *Physical Review B* **97**, 014201 (2018).
- [13] C. Lévesque, S. Roorda, F. Schiettekatte, and N. Mousseau, Internal mechanical dissipation mechanisms in amorphous silicon, *Physical Review Materials* **6**, 123604 (2022).
- [14] F. Puosi, F. Fidecaro, S. Capaccioli, D. Pisignano, and D. Leporini, Non-local cooperative atomic motions that govern dissipation in amorphous tantala unveiled by dynamical mechanical spectroscopy, *Acta Materialia* **201**, 1 (2020).
- [15] R. Hamdan, J. P. Trinastic, and H. Cheng, Molecular dynamics study of the mechanical loss in amorphous pure and doped silica, *The Journal of chemical physics* **141** (2014).
- [16] S. Khadka, A. Markosyan, K. Prasai, A. Dana, L. Yang, S. Tait, I. Martin, C. Menoni, M. Fejer, and R. Bassiri, Cryogenic mechanical loss of amorphous germania and titania-doped germania thin films, *Classical and Quantum Gravity* **40**, 205002 (2023).
- [17] K. Prasai, R. Bassiri, H.-P. Cheng, and M. M. Fejer, Annealing-induced changes in the atomic structure of amorphous silica, germania, and tantala using accelerated molecular dynamics, *physica status solidi (b)* **258**, 2000519 (2021).
- [18] M. Molina-Ruiz, Y. Rosen, H. Jacks, M. Abernathy, T. Metcalf, X. Liu, J. DuBois, and F. Hellman, Origin of mechanical and dielectric losses from two-level systems in amorphous silicon, *Physical Review Materials* **5**, 035601 (2021).
- [19] M. Molina-Ruiz, H. Jacks, D. Queen, T. Metcalf, X. Liu, and F. Hellman, Decoupling between propagating acoustic waves and two-level systems in hydrogenated amorphous silicon, *Physical Review B* **104**, 024204 (2021).
- [20] M. Molina-Ruiz, A. Markosyan, R. Bassiri, M. Fejer, M. Abernathy, T. Metcalf, X. Liu, G. Vajente, A. Ananyeva, and F. Hellman, Hydrogen-induced ultralow optical absorption and mechanical loss in amorphous silicon for gravitational-wave detectors, *Physical Review Letters* **131**, 256902 (2023).
- [21] H. Jacks, M. Molina-Ruiz, M. Weber, J. Maldonis, P. Voyles, M. Abernathy, T. Metcalf, X. Liu, and F. Hellman, Structural tunability and origin of two-level systems in amorphous silicon, *Physical Review Materials* **6**, 045604 (2022).
- [22] X. Liu, M. R. Abernathy, T. H. Metcalf, B. Jugdersuren, J. C. Culbertson, M. Molina-Ruiz, and F. Hellman, Comparing amorphous silicon prepared by electron-beam evaporation and sputtering toward eliminating atomic tunneling states, *Journal of Alloys and Compounds* **855**, 157431 (2021).
- [23] J. P. Trinastic, R. Hamdan, C. Billman, and H.-P. Cheng, Molecular dynamics modeling of mechanical loss in amorphous tantala and titania-doped tantala, *Physical Review B* **93**, 014105 (2016).
- [24] U. Seifert, Stochastic thermodynamics, fluctuation theorems and molecular machines, *Rep. Prog. Phys.* **75**, 126001 (2012).
- [25] C. Gardiner, *Handbook of Stochastic Methods for Physics, Chemistry and the Natural Sciences*, 2nd ed. (Springer, 1985).
- [26] F. Valiquette and N. Mousseau, Energy landscape of relaxed amorphous silicon, *Phys. Rev. B* **68**, 125209 (2003).
- [27] J. Tersoff, Modeling solid-state chemistry: Interatomic potentials for multicomponent systems, *Physical review B* **39**, 5566 (1989).
- [28] A. P. Thompson, H. M. Aktulga, R. Berger, D. S. Bolintineanu, W. M. Brown, P. S. Crozier, P. J. In't Veld, A. Kohlmeyer, S. G. Moore, T. D. Nguyen, *et al.*, LAMMPS—a flexible simulation tool for particle-based materials modeling at the atomic, meso, and continuum scales, *Computer Physics Communications* **271**, 108171 (2022).
- [29] V. L. Deringer, N. Bernstein, A. P. Bartók, M. J. Cliffe, R. N. Kerber, L. E. Marbella, C. P. Grey, S. R. Elliott, and G. Csányi, Realistic atomistic structure of amorphous silicon from machine-learning-driven molecular dynamics, *The journal of physical chemistry letters* **9**, 2879 (2018).
- [30] J. P. Doye, Network topology of a potential energy landscape: A static scale-free network, *Physical review letters* **88**, 238701 (2002).
- [31] X. F. Wang and G. Chen, Complex networks: small-world, scale-free and beyond, *IEEE circuits and systems magazine* **3**, 6 (2003).
- [32] D. Queen, X. Liu, J. Karel, H. Jacks, T. Metcalf, and F. Hellman, Two-level systems in evaporated amorphous silicon, *Journal of Non-Crystalline Solids* **426**, 19 (2015).
- [33] A. Fefferman, A. Maldonado, E. Collin, X. Liu, T. Metcalf, and G. Jernigan, Elastic measurements of amorphous silicon films at mk temperatures, *Journal of Low Temperature Physics* **187**, 654 (2017).
- [34] D. Khomenko, C. Scalliet, L. Berthier, D. R. Reichman, and F. Zamponi, Depletion of two-level systems in ultra-stable computer-generated glasses, *Physical review letters* **124**, 225901 (2020).
- [35] M. Luckabauer, T. Hayashi, H. Kato, and T. Ichitsubo, Decreasing activation energy of fast relaxation processes in a metallic glass during aging, *Physical Review B* **99**, 140202 (2019).

Supplemental Material for “Connected Network Model for the Mechanical Loss of Amorphous Materials”

I. ELASTIC ENERGY

In this section, we present an alternate derivation of the quality factor (15) based on the phase-lag of the average energy of the system. As discussed in the main text (2), the total energy of the system is the sum of the elastic energy and the average energy of the network

$$\mathcal{U}_{\text{tot}} = \mathcal{U}_{\text{elastic}} + \mathcal{U}_{\text{CN}} . \quad (\text{S1})$$

Substituting in the linear elastic energy Eq. (2), energy of the connected network Eq. (3), and assuming the approximation of Eq. (12) we have

$$\mathcal{U}_{\text{tot}} = \mathcal{V}C\epsilon_0^2 \sin^2(\omega t) + N \left[\mathbf{E}(0) + \frac{\epsilon_0\gamma_0}{2} \boldsymbol{\Gamma} \sin(\omega t) \right] \cdot \left[\mathbf{P}^{\text{eq}} - \frac{\beta\epsilon_0\gamma_0}{2} \mathbf{A} \sin(\omega t) - \frac{\beta\epsilon_0\gamma_0}{2} \mathbf{B} \cos(\omega t) \right] . \quad (\text{S2})$$

Expanding and collecting terms we have

$$\mathcal{U}_{\text{tot}} = N\mathbf{E}(0) \cdot \mathbf{P}^{\text{eq}} + \mathcal{U}_{\text{tot}}^{(1)} \sin(\omega t - \theta) + \mathcal{U}_{\text{tot}}^{(2)} \sin(\omega t - \phi) \sin(\omega t) , \quad (\text{S3})$$

for

$$\mathcal{U}_{\text{tot}}^{(1)} \equiv \frac{N\epsilon_0\gamma_0}{2} \sqrt{(\boldsymbol{\Gamma} \cdot \mathbf{P}^{\text{eq}} - \beta\mathbf{E}(0) \cdot \mathbf{A})^2 + (\beta\mathbf{E}(0) \cdot \mathbf{B})^2} \quad (\text{S4})$$

$$\theta \equiv \tan^{-1} \left[\frac{\beta\mathbf{E}(0) \cdot \mathbf{B}}{\boldsymbol{\Gamma} \cdot \mathbf{P}^{\text{eq}} - \beta\mathbf{E}(0) \cdot \mathbf{A}} \right] \quad (\text{S5})$$

$$\mathcal{U}_{\text{tot}}^{(2)} \equiv \frac{N\epsilon_0^2\gamma_0^2}{4} \sqrt{(\mathcal{V}C - \beta\boldsymbol{\Gamma} \cdot \mathbf{A})^2 + (\beta\boldsymbol{\Gamma} \cdot \mathbf{B})^2} \quad (\text{S6})$$

$$\phi \equiv \tan^{-1} \left[\frac{\beta N\gamma_0^2 \boldsymbol{\Gamma} \cdot \mathbf{B}}{4\mathcal{V}C - \beta N\gamma_0^2 \boldsymbol{\Gamma} \cdot \mathbf{A}} \right] . \quad (\text{S7})$$

The constant and linear terms average out to zero over one cycle and have no contribution to the overall mechanical loss. Substituting Eq. (13) and assuming $\mathcal{V}C \gg \beta N\gamma_0^2 \boldsymbol{\Gamma} \cdot \mathbf{A}/4$ we find

$$\tan \phi = Q^{-1} = \frac{\beta N\gamma_0^2}{\mathcal{V}C} \sum_{i,j,\ell} \Gamma_i M_{ij} \frac{\omega\tau_j}{[1 + (\omega\tau_j)^2]} M_{j\ell}^{-1} \Gamma_\ell P_\ell^{\text{eq}} . \quad (\text{S8})$$

The inverse quality factor can be expressed in terms of the phase lag of the system ϕ relative to the frequency of the oscillation ω : the mechanical loss results from the nonequilibrium, out of phase response of the system. The assumption $\mathcal{V}C \gg \beta N\gamma_0 \boldsymbol{\Gamma} \cdot \mathbf{A}/4$ is identical to the one made to arrive at equation (1) in Ref. [12] as shown in their equation (B6).

II. TLS DERIVATION

In this section we explicitly derive the mechanical loss for a TLS based on Eq. (15) for a two-state system. The transition rate matrix, Eq. (9), for a TLS consisting of state 1 and 2 is

$$R = k_0 \begin{bmatrix} -e^{-\beta(V-E_1)} & e^{-\beta(V-E_2)} \\ e^{-\beta(V-E_1)} & -e^{-\beta(V-E_2)} \end{bmatrix} . \quad (\text{S9})$$

Defining the energy asymmetry $\Delta = E_2 - E_1$ this simplifies to

$$R = k_0 e^{-\beta V} \begin{bmatrix} -1 & e^{\beta\Delta} \\ 1 & -e^{\beta\Delta} \end{bmatrix} , \quad (\text{S10})$$

where, without loss of generality, we have set $E_1 = 0$. This transition rate matrix has eigenvalues $\lambda_1 = 0$ and $\lambda_2 = -k_0 e^{-\beta V} (1 + e^{\beta \Delta})$ with corresponding eigenvectors $\mathbf{v}^{(1)} = [1, e^{-\beta \Delta}]$ and $\mathbf{v}^{(2)} = [-1, 1]$. The zero eigenvalue corresponds to the equilibrium distribution, so $\mathbf{P}^{\text{eq}} = \mathbf{v}^{(1)} / \sum_i v_i^{(1)}$.

The eigenvector matrix and its inverse are

$$M = \begin{bmatrix} 1 & -1 \\ e^{-\beta \Delta} & 1 \end{bmatrix} \quad (\text{S11})$$

and

$$M^{-1} = \frac{1}{1 + e^{-\beta \Delta}} \begin{bmatrix} 1 & 1 \\ -e^{-\beta \Delta} & 1 \end{bmatrix}. \quad (\text{S12})$$

setting $\mathbf{\Gamma} = [1, -1]$ (structures oscillate in opposite direction), substituting into Eq. (15), defining $\tau = -1/\lambda_2$ and summing over all TLS we arrive at Eq. (16). Note that the zero eigenvalue mode has no contribution to the mechanical loss.

III. SIMULATION DETAILS

In this section we provide additional simulation details. We perform molecular dynamics simulations in LAMMPS [28] using a Tersoff [27] potential to model silicon. By injecting random initial velocities, ten amorphous samples are prepared by rapidly melting diamond silicon from 100K to 4000K in 200ps, equilibrating at 4000K for 200ps, and subsequently cooling to 300K at a rate of 10^{11} K/s in the isobaric ensemble (target pressure $P=0$). Final amorphous configurations are found by energy minimization of the melt-quenched structure at constant volume.

With an average simulation box length of $27.43 \pm 0.01 \text{ \AA}$, the density of our samples is $2.261 \text{ g/cm}^3 \pm 0.001$. Using a cut off of 2.9 \AA the silicon atoms in the 10 samples have average coordination (with standard error) $c_3 = 0.42 \pm 0.08\%$, $c_4 = 95.8 \pm 0.2\%$, $c_5 = 3.8 \pm 0.2\%$, and $c_6 = 0.03 \pm 0.02\%$, where c_i is the percentage of the sample with coordination i . This corresponds to $\sim 4\%$ defects in our samples.

Once the samples have been prepared, we perform 100 random thermal searches per sample at 600K for 200ps. Every 0.1ps we save the structure of the system and the 2000 structures per search (200,000 per sample) are quenched to 0K providing an inherent structure of the system. Sequentially visited structures are considered as candidate connected pairs, and the atomic participation ratio (number of atoms involved in the transition) (18) and maximum atomic displacement between these pairs is calculated and used to filter out unlikely candidates as shown in Fig. S1.

In our data we observe two distinct regions in participation ratio- d_{max} space: pairs of structures with large participation ratio $\sim 10^3$ and small maximum atomic displacement and low participation ratio $\lesssim 100$ and comparatively large $d_{\text{max}} \gtrsim 0.1$. The former corresponds to all the atoms moving a very small distance and is likely the result of noise, while the latter involves relatively few atoms moving a larger distance.

We consider all the candidates with participation ratio < 100 and $d_{\text{max}} > 0.1$, then remove all duplicate pairs of atomic structures based on total root-mean squared atomic displacement of 10^{-4} \AA . From this filtered list, we perform nudged elastic band calculations with 32 intermediate structures to determine the transition path and barrier between the two states. If we find only a single maximum between the two states and the energy of that maximum is larger than the energy of both structures then we accept the pair as connected structures.

The full distribution of barriers and asymmetries between connected inherent structures is shown in Fig. S2. We observe a large peak in the barrier distribution at 0.2eV and a gap in barriers less than $\sim 0.1 \text{ eV}$. We observe a broad asymmetry distribution, with the main correlation to the energy barriers set by the maximum allowed value of $\Delta = 2(V - \bar{E})$.

To form the connected network, we calculate the root-mean squared total atomic displacement between all remaining inherent structures. If it is less than 10^{-4} \AA , then we assume they are the same inherent structure. This connects TLS together since distinct pairs of inherent structures (a TLS) often share one inherent structure. For example, the two TLS A-B and C-D would merge to form A-B-C if we determined state B and C were the same inherent structure.

The longitudinal component of the deformation potential is estimated from differences in stress $\Delta \sigma^{(ij)}$ between inherent structures i and j as suggested in ref. [12]:

$$\begin{aligned} (\gamma_0^L)^2 \Gamma_i^L \Gamma_j^L = & \frac{\mathcal{V}^2}{5} \left[(\Delta \sigma_{xx}^{(ij)})^2 + (\Delta \sigma_{yy}^{(ij)})^2 + (\Delta \sigma_{zz}^{(ij)})^2 \right] + \frac{2\mathcal{V}^2}{15} \left[\Delta \sigma_{xx}^{(ij)} \Delta \sigma_{yy}^{(ij)} + \Delta \sigma_{xx}^{(ij)} \Delta \sigma_{zz}^{(ij)} + \Delta \sigma_{yy}^{(ij)} \Delta \sigma_{zz}^{(ij)} \right] \\ & + \frac{4\mathcal{V}^2}{15} \left[(\Delta \sigma_{xy}^{(ij)})^2 + (\Delta \sigma_{xz}^{(ij)})^2 + (\Delta \sigma_{yz}^{(ij)})^2 \right]. \end{aligned} \quad (\text{S13})$$

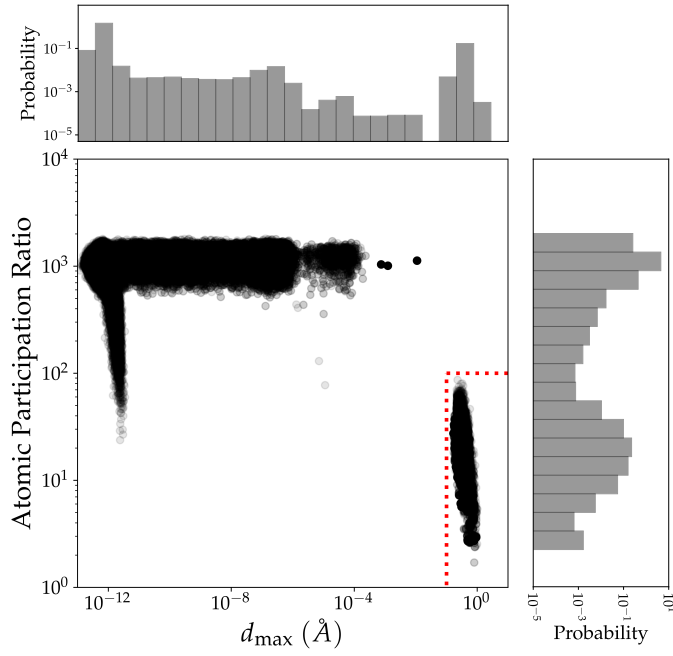


FIG. S1. Distribution of participation ratio and maximum atomic displacement d_{\max} between candidate connected inherent structures. The region enclosed by dotted red lines ($PR < 100$ and $d_{\max} > 0.1\text{\AA}$) are selected as likely candidates for being connected pairs.

Similar calculation yields the transverse component

$$\begin{aligned}
 (\gamma_0^T)^2 \Gamma_i^T \Gamma_j^T &= \frac{\mathcal{V}^2}{15} \left[(\Delta\sigma_{xx}^{(ij)})^2 + (\Delta\sigma_{yy}^{(ij)})^2 + (\Delta\sigma_{zz}^{(ij)})^2 \right] - \frac{\mathcal{V}^2}{15} \left[\Delta\sigma_{xx}^{(ij)} \Delta\sigma_{yy}^{(ij)} + \Delta\sigma_{xx}^{(ij)} \Delta\sigma_{zz}^{(ij)} + \Delta\sigma_{yy}^{(ij)} \Delta\sigma_{zz}^{(ij)} \right] \\
 &+ \frac{3\mathcal{V}^2}{15} \left[(\Delta\sigma_{xy}^{(ij)})^2 + (\Delta\sigma_{xz}^{(ij)})^2 + (\Delta\sigma_{yz}^{(ij)})^2 \right]. \quad (\text{S14})
 \end{aligned}$$

An example histogram of the product of longitudinal deformation potentials for one sample is shown in Fig. S3. States whose energy deforms in the same direction (increase or decrease energy) will have a positive product, and opposite directions a negative product. Similar to previous studies [13] we observe a fairly wide range of deformation potentials, with the product reaching up to 40eV^2 .

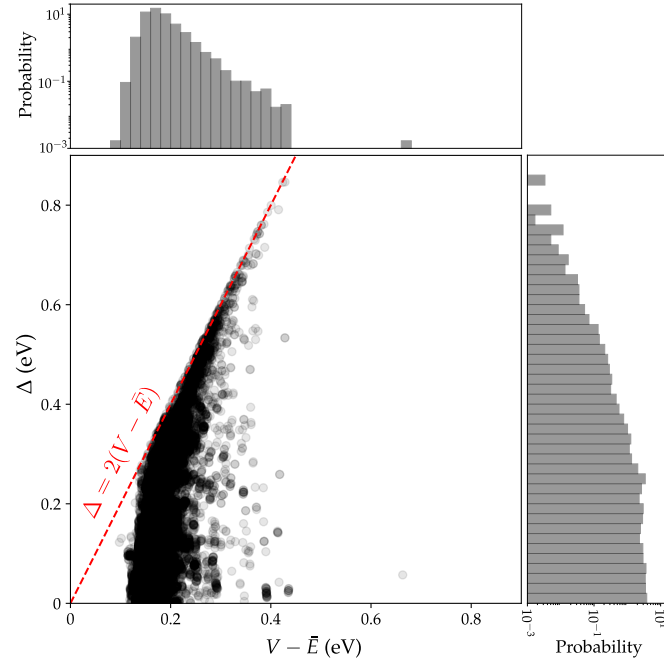


FIG. S2. Distribution of energy asymmetry and relative energy barrier $V - \bar{E}$ for $\bar{E} \equiv (E_i + E_j)/2$. Red dashed line shows the maximum possible asymmetry for a given barrier height $\Delta = 2(V - \bar{E})$.

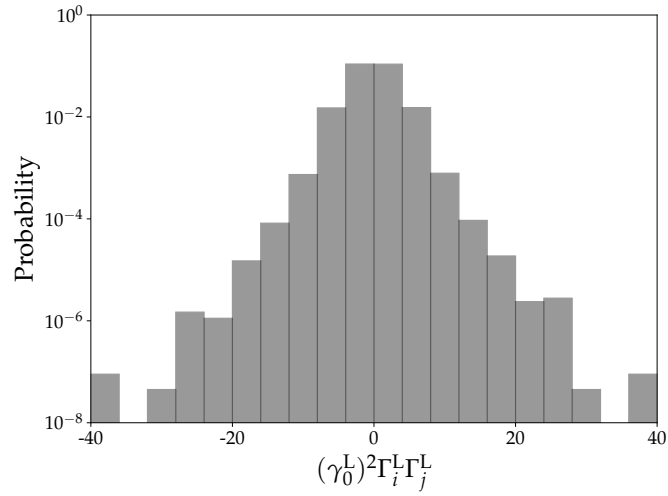


FIG. S3. Histogram of the longitudinal squared deformation potential (S13) in eV^2 for a single sample of amorphous silicon.